Smart Structures and Systems, *Vol. 17, No. 2 (2016) 275-296*
DOI: http://dx.doi.org/10.12989/sss.2016.17.2.275

A new configuration in a prosthetic knee using of hybrid concept of an MR brake with a T-shaped drum incorporating an arc form surface

Hassan Sayyaadi* and Seiyed Hamid Zareh[a]

School of Mechanical Engineering, Sharif University of Technology, Tehran, 11155-9567, Iran

(Received May 31, 2015, Revised November 27, 2015, Accepted December 9, 2015)

Abstract. This paper focuses on developing a new configuration on magnetorheological (MR) brake damper as prosthetic knee. Prosthetic knee uses magnetic fields to vary the viscosity of the MR fluid, and thereby its flexion resistance. Exerted transmissibility torque of the knee greatly depends on the magnetic field intensity in the MR fluid. In this study a rotary damper using MR fluid is addressed in which a single rotary disc will act as a brake while MR fluid is activated by magnetic field in different walking gait. The main objective of this study is to investigate a prosthetic knee with one activating rotary disc to accomplish necessary braking torque in walking gait via T-shaped drum with arc surface boundary and implementing of Newton's equation of motion to derive generated torque at the inner surface of the rotary drum. For this purpose a novel configuration of a T-shaped drum based on the effects of a material deformation process is proposed. In this new design, the T-shaped disc will increase the effective areas of influences in between drum and MR fluid together and the arc wall crushes the particles chains (fibrils) of the MR fluid together instead of breaking them via strain in a conventional MR brake. To verify the proposed MR brake, results of the proposed and conventional MR brakes are compared together and demonstrated that the resisting torque of the proposed MR brake is almost two times greater than that of the conventional brake.

Keywords: prosthetic knee; magnetorheological (MR) brake; T-shaped drum

1. Introduction

Magnetorheological (MR) fluids are those which act magnetically sensitive in rheological properties. MR fluids are now being developed and applied to many actuators such as automobile shock absorbers, dynamic positioning in offshore structures, different kinds of dampers' applications, power transmission clutches, machinery brake systems (Carlson *et al.* 2000, Zhou *et al.* 2012, Wereley *et al.* 2008, Dyke *et al.* 1998, Zareh *et al.* 2011, Xu *et al.* 2012, Li *et al.* 2003, Nam *et al.* 2009, Rossa *et al.* 2014), prosthetic limbs and biomechanics (Jonsdottir *et al.* 2009, Naito *et al.* 2009, Jonsdottir *et al.* 2010, Carlson *et al.* 2001, Gudmundsson *et al.* 2011, Zite *et al.* 2006) and rehabilitation and exercises devices (Liu *et al.* 2006, Avraam *et al.* 2010). Reported advantages of these MR fluid devices include; easy to construct, low operational power density,

*Corresponding author, Associate Professor, E-mail: sayyaadi@sharif.edu
[a] Ph.D. Student, E-mail: zareh@mech.sharif.edu

http://www.techno-press.org/?journal=sss&subpage=8 ISSN: 1738-1584 (Print), 1738-1991 (Online)

providing high damping force, and fast dynamic responses. Rotary MR dampers are not in use as extensive as the linear MR dampers, many types and classes of rotary MR dampers have been developed for different purposes. In the beginning of its applications, the term of MR brake was more commonly used than that of rotary MR damper, since the early intentions of the device development were only as braking devices. MR brakes, as one of the most common application branches of rotary MR damper, have been discussed in many literatures (Liu *et al.* 2006, Avraam *et al.* 2010, Nguyen *et al.* 2011). Most common types of variable torque brakes that have been employed in prosthetic knees in the past are classified to: dry friction brakes and viscous torque brakes. Each of these technologies, as conventionally practiced in the field of prosthetics, can pose certain disadvantages. For instance, viscous torque brakes are at risk of leakage in hydraulic fluid. Frictional pads in the dry friction brakes tend to wear and change the frictional characteristics.

MR prosthetic knee can overcome to the most of the above mentioned technological limitations (Jonsdottir *et al.* 2009). One of the famous prosthetic knees is manufactured by the company Ossur Inc. based on the rotary brake, recently. Flexion resistance of the knee is generated using of magnetic fields to vary the viscosity of the MR fluid. MR fluid is activated only when individual needs to produce the resistance force. Ossur prosthetic knee can support for lightweight patients only and to deal with this limitation, (Jonsdottir *et al.* 2009, Gudmundsson *et al.* 2011) researches are carried out to increase the maximum accessible torques, to make it suitable to be able to support heavier patients apparently.

Due to the limitation in overall size of the apparatus to be fitted to the human body, overall dimensions and weight are restricted so that in newly designs, using multi layers discs in MR brake (about 63 very thin blades) are reported. Gap between the disc blades, where the fluid resides, is of the very small sizes compared to the width of the blades (about 30 μm). They selected this gap to increase on state torque; therefore they had to design a new bimodal MR fluid just for their device (Gudmundsson *et al.* 2011). Their MR fluid is composed of nano and micron particles. One of the most important drawbacks of the device is its high sensitivity to impact because of their small tolerances in blades gaps. Second disadvantages is its high off state torque which leads to low flexibility in flexion of the knee gait and the third one is high cost of the specific MR fluids. Also, base on the implicational sizes, geometries, biomechanical features, and other specifications and limitations (dimension, size, weight, etc.) the other MR brake types like disk type and drum type cannot generate the required braking torque. For example a disk type with 120 mm radius and 12 kg weight can produce braking torque only 23Nm (Park *et al.* 2008). Therefore these types cannot be used for this application.

The goal of this work is to overcome the above drawbacks using of a new magnetorheological brake (MRB) damper configuration to increase the maximum obtainable torque by one blade, because the proposed configuration (T-shape drum) has more area to generate braking torque with respect the other types with the same overall size. The effort to improve the performance of the proposed prosthetic knee is a hybrid concept of a T-shaped drum with arc boundary by magnetic circuit using both axial and radial magnetic flux, so that the achievable braking torque is multiplied. Recent studies of the MR brake after 2010 have discussed the hybrid type of MR brake (Nguyen *et al.* 2011, Nguyen *et al.* 2012a, Nguyen *et al.* 2012b) because drum and disc type of MR brakes have reached bottleneck. The term hybrid refers to combination of radial flux direction (usually in drum type MR brake) and axial flux direction (usually in disc type of MR brake).

Several configurations have been used for hybrid type of MR brakes. One of the most effective is T-shaped (Nguyen *et al.* 2012b) which is selected for this study. The brake has smooth outer face; therefore to achieve high braking torque it needs large radius.

To reach more braking torque, rotary disk type of MR brake incorporating with a waveform disk is designed by Nam *et al.* (2009) as the only research in this field. They used curved element with slab method to propose deformation modeling of MR fluid in solid state. Their mathematical model is very complicated and it is not fully compatible with the actual model in the rolling process, because some neglected parts and some integral approximation of this model have tremendous effects on the model.

Although there have been a large number of research studies on the design and application of MRBs and various types of configuration have been proposed, but no one utilized hybrid concept with arc boundary for prosthetic knee. Therefore, in current research, strip drawing method with trapezoid element is used for simplicity and more compatible with deformation model of MR fluid in solid state (Hosford *et al.* 2007). Also, in this study, two coils are placed at the bottom and top of the two ends of the flange of the T-shaped drum. Unlike the location of coils in (Nguyen *et al.* 2012a, Nguyen *et al.* 2012b), using of these locations, torque across the two lateral sides of the T-flange is achievable.

Base on the limitations (size, dimension and weight of the brake), the conventional T-shaped MRB or a disc type waveform, cannot solely do the task. Thus, to promote torque to achieve the desired flexion/extension in the knee (maximum required torque for a heavy amputee, weighting 90 kg is 36 Nm (Kirkwood *et al.* 2007)), arc surface is considered for the outer surface of the T-flange. Consequently, the main contribution of this work is to focus on developing a novel configuration of MR brakes with one disc as the prosthetic knee using of hybrid concept with the strip drawing method with trapezoid element. Also, to obtain the governing equation of motion of MR fluid in the inner of the drum to calculate generated torque, unlike previous works, Newton's equation of motion is applied for the case of an MR fluid confined between two concentric cylinders. The proposed configuration utilizes both axial and radial magnetic flux and the effects of a material deformation process to generate braking force. A comparison between the proposed and the conventional data are presented.

2. Proposed prosthetic knee

In this research, the proposed configuration of the MR brake as prosthetic knee (see Fig. 1) with its geometric dimensions is shown in Fig. 2. The T-shaped drum is connected to the inner house (rotor) and the outer house (stator). The stator and the rotor are separated from each other using MR fluid.

Fig. 1 An MR prosthetic knee joint

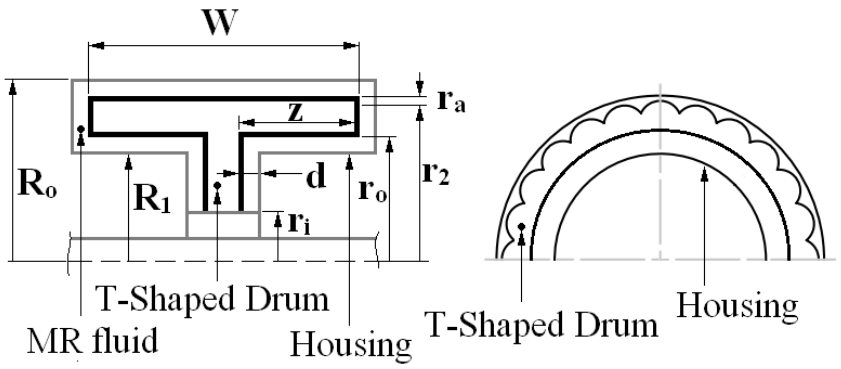

Fig. 2 Configuration of the hybrid T-type MRB

The rotor is connected to the amputee's lower part of the leg (below the knee) and the stator is connected to the amputee's residual limb. This mechanism is generating the relative motion between the two parts. The gap between the drum and housing, where the fluid resides, is small and it is larger than the proposed disc type in (Jonsdottir *et al.* 2009). This larger gap leads to more freely motion without a magnetic field. In a prosthetic knee joint, the field-induced characteristics and the off-state characteristics of the MR fluid are of equal importance (Gudmundsson *et al.* 2011). Under the effect of a magnetic field, the on-state shear yield stress determines how rigid the knee joint is, and the off-state viscosity determines how flexible it is. As the knee rotates into flexion or extension, when a magnetic field is applied, the drum shears the particle chains to create resistance.

When currents are applied to the coils, a mutual magnetic circuit which is shown in Fig. 3 is generated. The coils were wound in directions opposite to each other so that the flux lines would be added up in the gaps. Due to the magnetic flux of the coils, a large braking torque of the brake is expected. This magnetic circuit produces an induced stress of MR fluid in the gaps at the inner and outer faces of the T-flange, lateral sides of the T-flange and two sides of the T-leg.

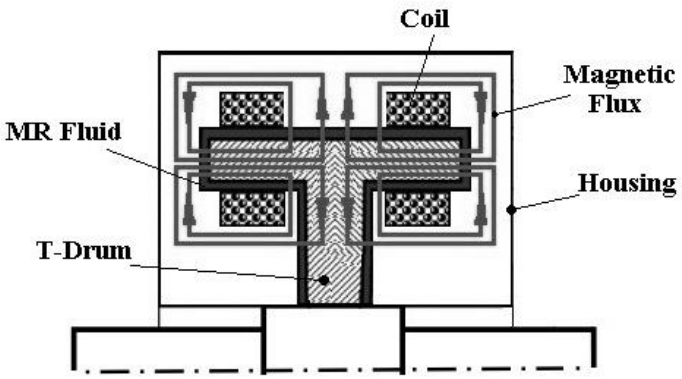

Fig. 3 Schematic of the flux lines

3. Torque in a radial duct

The generated torque from the MR fluid in radial duct (T_1) can be expressed by

$$T_1 = 2\pi \int_{r_i}^{r_o} r^2 \tau_f dr \tag{1}$$

where r_i and r_o are the inner and outer radius of the T-leg. τ_f is the shear stress acting on the MR fluid. When a magnetic field is applied, the fluid can be characterized by the Bingham's plastic model (Spencer *et al.* 1997).

$$\tau_f = \tau_y(H) + \eta\dot{\gamma} \tag{2}$$

where τ_y is the yield stress of the MR fluid which is variable to magnetic field strength H and η is the MR fluid viscosity when no magnetic field applied, $\dot{\gamma}$ is the shear rate. Because the gap size is very small, the shear rate of the MR fluid in the gap can be approximately determined as follows

$$\dot{\gamma} = \frac{r\omega}{d} \tag{3}$$

where ω is the angular speed and d is the gap size. A rough estimate of the rotating speed from a typical design of the knee (Gudmundsson *et al.* 2011) gives a 5 rpm. Combining Eq. (2) and (3) with Eq. (1), gives the following equation

$$T_1 = 2\pi \int_{r_i}^{r_o} r^2 [\tau_y(H) + \eta \frac{r\omega}{d}] dr \tag{4}$$

In order to facilitate the calculation, it is assumed that in the gap, the magnetic density is constant (Nguyen *et al.* 2012b).

$$T_1 = \frac{2\pi\tau_y(H)}{3}(r_o^3 - r_i^3) + \frac{2\pi\eta r_o^4}{4d}[1 - (\frac{r_i}{r_o})^4]\omega \tag{5}$$

Similar to the torque in the radial duct, the torque in a lateral side of the T-flange (T_2) can be determined by

$$T_2 = \frac{2\pi\tau_y(H)}{3}(r_2^3 - r_o^3) + \frac{2\pi\eta r_2^4}{4d}[1 - (\frac{r_o}{r_2})^4]\omega \tag{6}$$

where r_2 is the upper edge radius of the T-flange.

4. Torque at the inner face of the T-flange

In previous works (Nguyen *et al.* 2011, Nguyen *et al.* 2012a, Nguyen *et al.* 2012b), to obtain induced torque at the inner face, they integrated shear stress on the face. But here, Newton's equation of motion is applied to achieve the governing equation of motion of MR fluid in inner

face of the T-flange (Fig. 4). Due to the geometry of the brake, cylindrical coordinate system is used. The equation of motion of a fluid particle is

$$\rho\vec{g} - \vec{\nabla}p + \vec{\nabla}.\tau_{ij} = \rho\frac{d\vec{v}}{dt} \tag{7}$$

where

$$\vec{g} = g_r\vec{e}_r + g_\theta\vec{e}_\theta + g_z\vec{e}_z \tag{8}$$

$$\vec{v} = v_r\vec{e}_r + v_\theta\vec{e}_\theta + v_z\vec{e}_z \tag{9}$$

v and g are the velocity and gravity fields; respectively, ρ is the fluid density, ∇p is the pressure gradient, and τ_{ij} is the *ijth* component of the stress tensor. The equation of motion in θ direction results

$$\begin{aligned} &-\frac{1}{r}\frac{\partial p}{\partial\theta} + \frac{\partial\tau_{r\theta}}{\partial r} + \frac{1}{r}\frac{\partial\tau_{\theta\theta}}{\partial\theta} + \frac{\partial\tau_{\theta z}}{\partial z} + \frac{2}{r}\tau_{r\theta} + \rho g_\theta \\ &\quad = \rho\left(\frac{\partial v_\theta}{\partial t} + v_r\frac{\partial v_\theta}{\partial r} + \frac{1}{r}v_\theta\frac{\partial v_\theta}{\partial\theta} + v_z\frac{\partial v_\theta}{\partial z} + \frac{1}{r}v_r v_\theta\right) \end{aligned} \tag{10}$$

Assuming steady-state flow, symmetry, no velocity in the axial direction and neglecting the gravitational effects, the above equation is simplified to

$$\frac{\partial\tau_{r\theta}}{\partial r} + \frac{2}{r}\tau_{r\theta} = 0 \tag{11}$$

$$\frac{\partial\tau}{\partial r} + \frac{2}{r}\tau = 0 \tag{12}$$

$$\frac{\partial\tau}{\tau} = -2\frac{\partial r}{r} \tag{13}$$

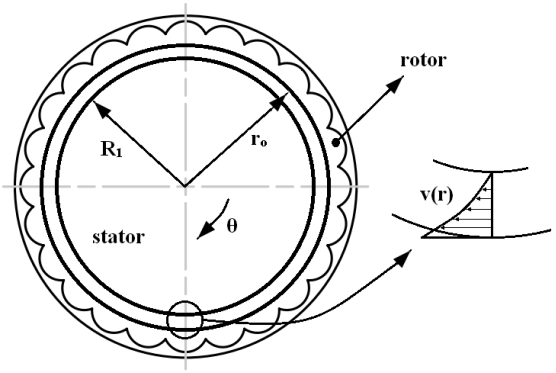

Fig. 4 Schematic of the cross section of the brake and the velocity profile

For simplicity τ is used instead of $\tau_{r\theta}$. The equation of shear stress using above differential equation is as a function of r.

$$\tau = \frac{c_1}{r^2} \tag{14}$$

where c_1 is a constant which is determined via the boundary conditions. The velocity increase from zero at R_1 to $r_o\omega$ at r_o; therefore, like Couette flow, the shear rate is

$$\dot{\gamma} = \frac{dv}{dr} - \frac{v}{r} \tag{15}$$

$$\tau = \tau_y + \eta(\frac{dv}{dr} - \frac{v}{r}) \tag{16}$$

By combining Eq. (14) with Eq. (16) and rearranging

$$\int_{\omega_0}^{\omega} d\omega = \int_{R_1}^{r} \frac{1}{r}(\frac{c_1}{\eta r^2} - \frac{\tau_y}{\eta})dr \tag{17}$$

The velocity sketch will be obtained by using integration and the boundary conditions.

$$v(r) = r\omega = r[-\frac{c_1}{2\eta r^2} + \frac{\tau_y \ln r}{\eta} + c_2] \tag{18}$$

$$c_1 = \frac{2R_1^2 r_o^2[\tau_y \ln \frac{r_o}{R_1} + \eta\omega_o]}{R_1^2 - r_o^2} \tag{19}$$

$$c_2 = \frac{r_o^2[\tau_y \ln \frac{r_o}{R_1} + \eta\omega_o]}{\eta(R_1^2 - r_o^2)} + \frac{\tau_y}{\eta}\ln R_1 \tag{20}$$

The shear stress on the inner surface of the T-flange using Eq. (14) is used to calculate the torque equation

$$dF_3 = \tau dA = \tau(r_0)2\pi r_0 dz \tag{21}$$

$$dT_3 = r_o dF_3 \tag{22}$$

$$T_3 = -\frac{4\pi R_1^2 r_o^2[\tau_y \ln \frac{r_o}{R_1} + \eta\omega_o]}{r_o^2 - R_1^2} z \tag{23}$$

where z is the width of one inner face. The minus sign is because the torque generated by MR fluid that is a restraining torque and opposes the motion of the rotor.

5. Torque at the outer face of the T-flange

5.1 Fundamental approach

The arc surface of the rotary disk which is shown in Fig. 4 not only creates the dynamic effect from its cylindrical form, but also creates many local MR zones. This boundary changes the direction of the magnetic fibrils. The boundary redistributes and concentrates the magnetic flux on the MR zones but does not obstruct motion (Fig. 5). At these areas, the magnetic field intensity and the magnetic flux density are increasing. With the contacted arc, most of the generated braking torque is from the deformational process of an MR fluid under the drawing motion.

Under the applied magnetic field, a MR fluid is considered to be a solid material with a variable yield stress. When the magnetic field is applied, the drawing force must achieve a critical value to create motion. This value is the minimum critical force needed to break the hardened MR zone. When this process occurs, the deformation stress reaches the yield stress, which is the shear stress of the MR fluid.

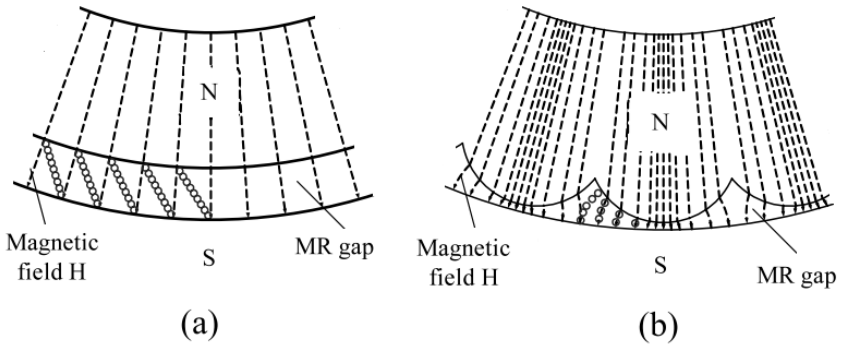

Fig. 5 Magnetic field distribution of brake damper. (a) Conventional MR gap and (b) Proposed MR gap

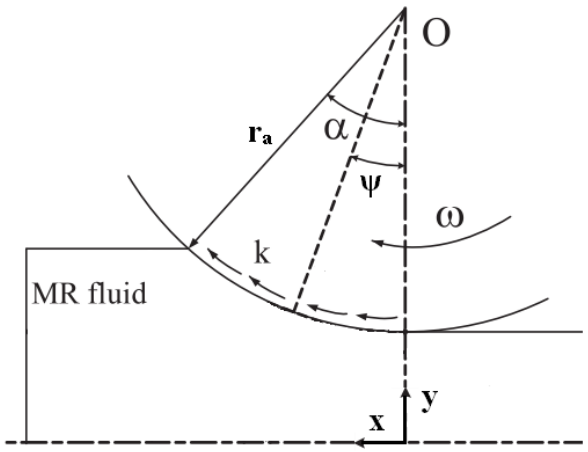

Fig. 6 Deformation model for the resistance force of MR fluid in solid state

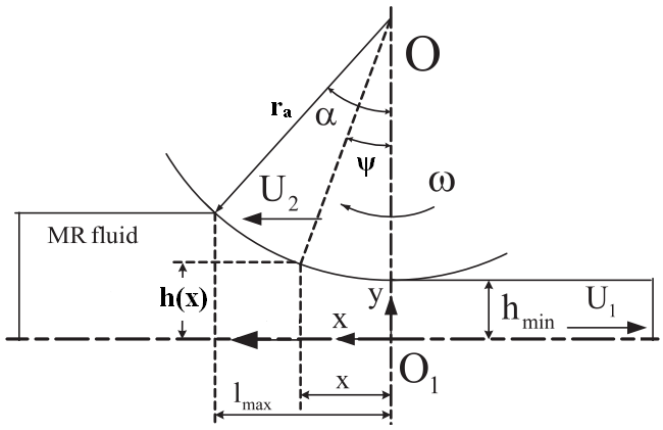

Fig. 7 Hydrodynamic model for the hydrodynamic resistance force

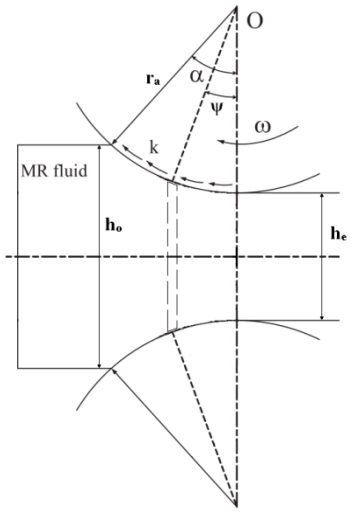

Fig. 8 Double model for the first part calculation

The generated torque from the outer surface of the proposed brake which is shown has two parts. The first one is the deformation model (Fig. 6) and the second one is the hydrodynamic model (Fig. 7). Where α is slit angle in the rotary disk and r_a is the radius of contacted arc. The pressure at the input and output gates of MR fluid in the working zone is zero. U_1 and U_2 are the relational speed in the slide motion between the arc and housing.

The double model as shown in Fig. 8 is considered on the axis of symmetry for generating the first part. This axis is assumed as the magnetic pole of the housing and the MR fluid will now move together with the housing with a very small elastic distortion. This double model is compatible with the process of hot deformation of metal material under the drawing force (Hosford *et al.* 2007) with strip drawing method.

5.2 Mathematical model of the proposed approach

Fig. 9 shows the differential strip drawing element. p and k are the normal stress and shear stress on the arc surface, respectively. An x direction force balance gives

$$(\sigma_x + d\sigma_x)(h+dh)W + 2pW\tan\psi dx + k\cos\psi W dx = \sigma_x Wh \tag{24}$$

Simplifying and neglecting second order differentials

$$\sigma_x h + \sigma_x dh + h d\sigma_x + 2p\tan\psi dx + k\cos\psi dx = \sigma_x h \tag{25}$$

Using the geometrical relationship $2dx=dh/\tan\psi$ and the yield condition σ_x-$p=2k$:

$$(2k+p)dh + hdp + pdh + k\cos\psi\cot\psi dh = 0 \tag{26}$$

Above equation is integrated to the Eq. (27). Here it is assumed that k is the yield stress in pure shear $k = \tau_y(B)$ and depends on the characteristic of an MR fluid and the magnetic field $B(T)$

$$\frac{p}{k} = \frac{(2+\cos\psi\cot\psi)}{2}[(\frac{h_o}{h_e})^2 - 1] \tag{27}$$

Let F_p be the transmitted horizontal force from an external force through the rotary disk, acting on the MR zone which is explained and solved in the following equations

$$F_p = 2\left(\int_0^{\alpha} r_a p\sin\psi d\psi + \int_0^{\alpha} r_a k\cos\psi d\psi\right) \tag{28}$$

$$F_p = 2\left(\frac{r_a k}{16}[(\frac{h_o}{h_e})^2 - 1]\left(\sin 2\alpha + 2\alpha - 8\cos\alpha + 8\right) + r_a k\sin\alpha\right) \tag{29}$$

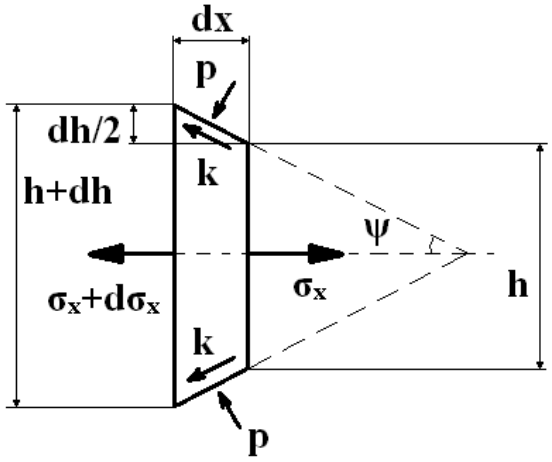

Fig. 9 Element of MR fluid in strip drawing method for force balance

where $\alpha(rad)$ is the angle of the effective hardened MR zone. The resistance force F_d acting on the rotary disk is

$$F_d = \frac{1}{2} F_p \tag{30}$$

In the Fig. 7, the friction force is the remainder resistance force. The friction force is a result of the MR fluid prevention when the arc moves inside it. These formulations are calculated for a single contacted arc using the theory of hydrodynamic lubrication (Pinkus 1961). The generalized Reynolds equation is used to calculate the resistance force.

$$\nabla.\left[\left(\frac{\rho y^3}{\eta}\right)\nabla p\right] = 12\frac{\partial(\rho y)}{\partial t} + 6\nabla.(\rho y U) \tag{31}$$

For incompressible lubricants ($\rho=const$), constant speed ($U=const$) and the fixed geometrical conditions, the generalized form can be reduced to the following equation

$$\frac{\partial}{\partial x}\left(\frac{h(x)^3}{\eta}\frac{\partial p}{\partial x}\right) = -6U\frac{\partial h(x)}{\partial x} \tag{32}$$

Based on the shear equation of lubrication in (Pinkus 1961), the velocity profile is

$$u = \frac{1}{2\eta}\frac{\partial p}{\partial x} y(y - h(x)) + \frac{y - h(x)}{h(x)} U \tag{33}$$

Using of Bingham model and the velocity profile, the shear stress in the MR fluid with the fixed coordinated is expressed in

$$\tau = \tau_0(B) + \eta\left[\frac{1}{2\eta}\frac{\partial p}{\partial x}(2y - h(x)) + \frac{1}{h(x)}(U_2 - U_1)\right] \tag{34}$$

where the speed $U_1=0$ and $U_2=U$. To create an initial motion in the fluid flow, the viscous shear stress ($\tau_{y,v}=\eta(\partial u/\partial y)$) must overcome the Coulomb shear stress ($\tau_{y,c}=\tau 0(B)$) which is often larger than the viscous shear stress. The hydrodynamic resistance force per unit width generated by the Coulomb shear stress is

$$F_{\tau(B)} = \tau_0(B) l_{\max} \tag{35}$$

Here l_{max} is obtained where the pressure profile is zero. Now, to calculate viscous shear stress, first the pressure gradient must be obtained in the region between the arc and housing. There is a significant pressure gradient only in the region close to the minimum film thickness (Harnoy 2002). The surface velocity of the cylinder is not parallel to the x direction and it has a normal component V_2. The surface velocities on the rotating cylinder surface are

$$U_2 = \omega(r_a + r_2)\cos\alpha \approx \omega(r_a + r_2) \tag{36}$$

$$V_2 \approx \omega(r_a + r_2)\frac{\partial h}{\partial x} \tag{37}$$

For a small α, approximate that $\cos\alpha \approx 1$. At the same time, the velocity of the housing is zero. Substituting these values with the right side of Reynolds equation and integration, the pressure gradient yields

$$\frac{dp}{dx} = 6\eta\omega(r_a + r_2)\frac{h(x) - h_0}{h(x)^3} \tag{38}$$

where $h(x)$ is the film thickness. The unknown constant h_0, (constant of integration) is equal to h_{min}. The film thickness in the clearance between a flat plate and a cylinder is given by

$$h(\theta) = h_{mm} + r_a(1 - \cos\psi) \tag{39}$$

where ψ is a cylinder angle measured from the minimum film thickness at $x=0$. Since the minimum clearance, h_{min}, is small (relative to the cylinder radius), the pressure is generated at a region close to the minimum film thickness (Harnoy 2002). For a small ratio of x/r_a, the equation of the clearance, $h(x)$, can be approximated by a parabolic equation. The following expression is obtained by expanding above equation for $h(x)$ into a Taylor series and truncating terms that include powers higher than $(x/r_a)^2$. In this way, the expression for the film thickness, $h(x)$, can be approximated by

$$h(x) = h_{min} + \frac{x^2}{2r_a} \tag{40}$$

The hydrodynamic resistance force generated from the viscous shear stress per unit width is expressed by

$$F_\eta = 2\eta r_a \left(\frac{9\omega\lambda x}{4(2h_{\min} r_a + x^2)} - \frac{3\omega h_{\min} r_a \lambda x}{(2h_{\min} r_a + x^2)^2} - \frac{3\omega\lambda - 4u}{\sqrt{32 h_{\min} r_a}} \arctan\left(\frac{x}{\sqrt{2h_{\min} r_a}} \right) \right) \tag{41}$$

where

$$\lambda = r_a + r_2 \tag{42}$$

The general resistance force per unit width for one contacted arc is the sum of resistance forces in Eq. (30), (35) and Eq. (41). Here, the effect of mechanical frictions such as a bearing friction and seal friction is neglected.

$$F_r = F_d + F_\tau + F_\eta \tag{43}$$

The achievable torque from outer face of the proposed MR brake is shown in Eq. (44) and denoted by T_{4p}.

$$T_{4p} = r_2 W N_a \Gamma_a F_r \tag{44}$$

where N_a is the number of the arc, W is the width of outer face and Γ_a is the effective coefficient of the arc's width. The effective coefficient Γ_a of the arc's width is the percent of hardened MR fluid in the MR zone following the width direction under the magnetic field, which joined to create the real resistance force. Here, Γ_a is considered 0.8 (Nam *et al.* 2009). The total output torques of the

above-mentioned structures for the proposed MR brake is shown in the following equation

$$T_{total\,p} = 2T_1 + 2T_2 + 2T_3 + T_{4p} + T_b + T_o \tag{45}$$

The torque due to friction in bearings, T_b, is assumed to be 0.8 Nm at an angular speed of 5.2 rpm, and the friction in oil seals, T_o, is assumed to be 0.8 Nm, at the same angular speed. In this study, just for simulation, the torque due to friction in bearings and the friction in oil seals are considered. Special issues in manufacturing process like the clearance, bearing selection or seal problem will be considered for the manufacturing process in the further researches.

5.3 Torque at the outer face of the conventional brake

The torque in the outer face without arc for conventional brake, T_{4c}, similarly is like the torque in the inner face, T_3.

$$T_{4c} = -\frac{4\pi R_o^2 r_2^2 [\tau_y \ln \frac{R_o}{r_2} + \eta\omega_o]}{r_2^2 - R_o^2} W \tag{46}$$

The total output torques of the conventional structures without arcs for the brake is shown in the following equation.

$$T_{total\,c} = 2T_1 + 2T_2 + 2T_3 + T_{4c} + T_b + T_o \tag{47}$$

6. Magnetic circuit design

The configuration which is shown in Fig. 10 corresponds to the condition where an electromagnet is used to control the viscosity of the MR fluid. The minimum viscosity of the MR-fluid is when no current applied to the coil. Assuming there is uniform flux densities inside the magnetic circuit and neglecting the leakage flux.
where, Φ is the magnetic flux and N_w is the number of coil turns. The equivalent electric circuit is shown at Fig. 11. $\Re_{MR}$ and $\Re_{iron}$ are the MR fluid and iron reluctance, respectively. The equivalent Kirchhoff's voltage law gives

$$N_w I = (\Re_{MR} + \Re_{iron})\Phi \tag{48}$$

leading to

$$\Phi = \frac{N_w I}{\Re_{MR} + \Re_{iron}} \tag{49}$$

$$\Phi = \frac{N_w I}{(l_{MR} / \mu_{MR} A_{MR}) + (l_{iron} / \mu_{iron} A_{iron})} \tag{50}$$

which is equivalent to

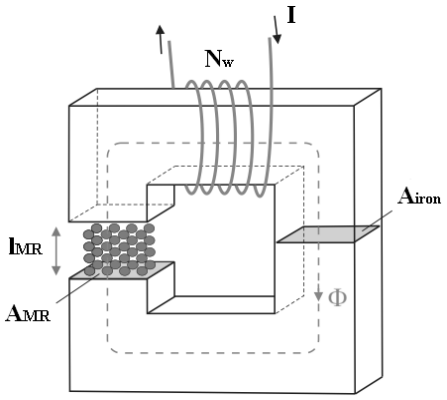

Fig. 10 Magnetic core with MR fluid filled gap

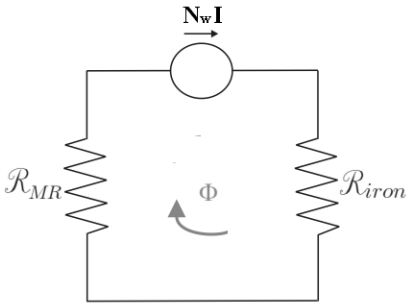

Fig. 11 Electric equivalence magnetic circuit

$$H_{MR} = \frac{\Phi}{\mu_{MR} A_{MR}} = \frac{N_w I}{l_{MR} + l_{iron}(\mu_{MR} / \mu_{iron})(A_{MR} / A_{iron})} \tag{51}$$

where μ_{MR} and μ_{iron} are relative permeability of the MR fluid and the iron (typical values are: iron=5000; MR fluid=5) and l_{iron} is the length of the magnetic path. It is however important to note that $\mu_{iron} \approx 1000\mu_{MR}$. Consequently, provided that l_{iron} is not too large and that the MR fluid and soft-steel core sections are in the same range, Eq. (51) can be simplified to

$$H_{MR} = \frac{\Phi}{\mu_{MR} A_{MR}} = \frac{N_w I}{l_{MR}} \tag{52}$$

Fringing of magnetic flux appears at the interface between the gap and the soft iron core which is shown in Fig. 12(a).

In order to take the effect of fringing into account during the design process, an effective gap section which is shown in Fig. 12(b) (A'_{MR}) is considered.

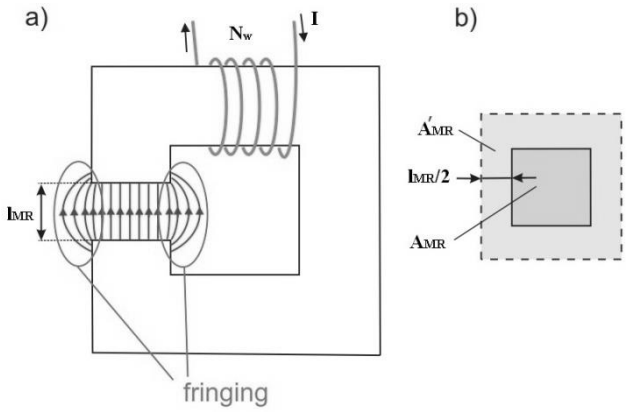

Fig. 12 Fringing of magnetic flux lines (a) interface with a MR fluid gap and (b) an effective gap section

7. Results

In this research, it is assumed that the rotor and stator of the MRBs are made of commercial silicon steel, aluminum and the considered commercial MRF is MRF-132DG as a reference fluid. The shear yield stress as a function of the magnetic flux density for the MR fluid manufactured by the company Lord Inc. is shown in Fig. 13. The B-H curves for the MR fluid and the drum are also shown in Fig. 14.Yield stress curve is fitted with an analytical curve described by

$$\tau_y(B) = \alpha + \beta\cos(\pi.B) + \zeta\sin(\pi.B) \tag{53}$$

Values of the fitted parameters α, β and ζ are given in Table 1.

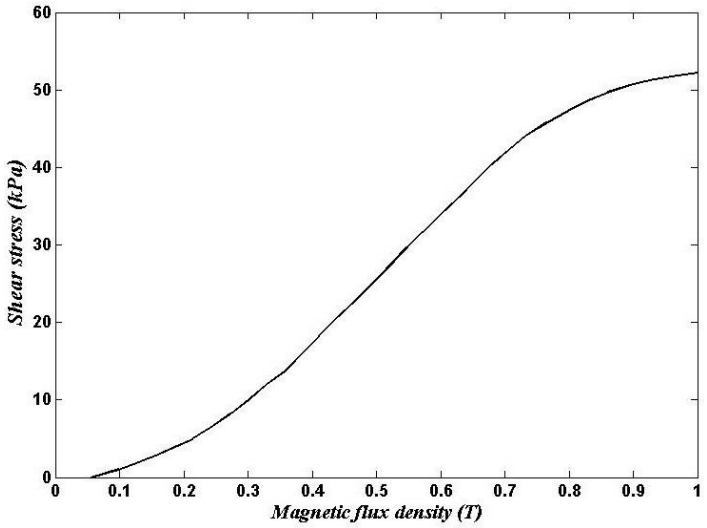

Fig. 13 Shear yield stress as function of magnetic flux density

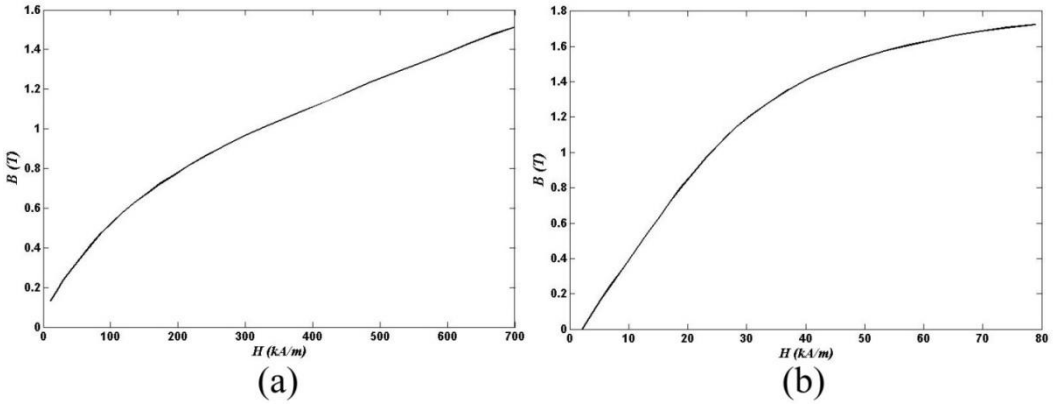

Fig. 14 B-H curve for the MRF-132DG (a) and the drum (b)

Table 1 Rheological parameters of the MRF

parameter	value
α	26700 Pa
β	-26400 Pa
ζ	-200 Pa

It can be seen that the drum has a more linear magnetic property compared to the MR fluid when the applied magnetic field is small. As the magnetic field increases, a gradual magnetic saturation is observed and consequently, the MR fluid yield stress is saturating (Fig. 13). As shown in Fig. 15, the magnetic flux redistributes to and concentrates on the MR zones using of arc surface. At these zones, the magnetic field intensity, *H*, is increased.

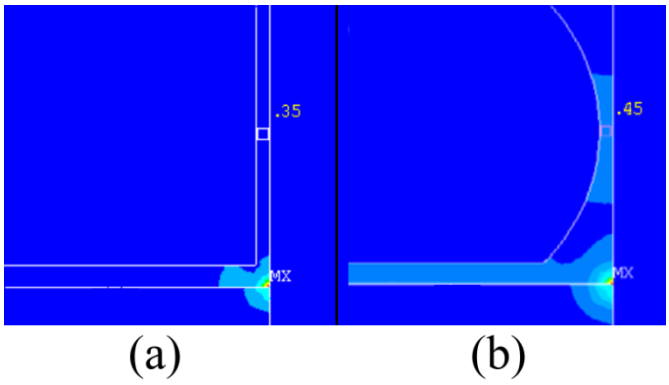

Fig. 15 Magnetic field intensity of the conventional (a) and proposed case (b)

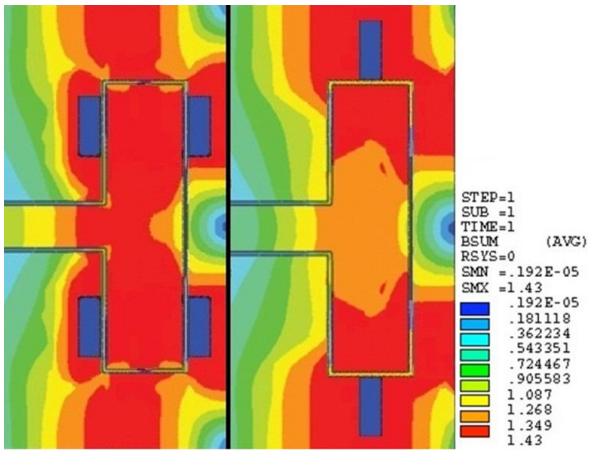

Fig. 16 Magnetic flux density in the MR brake using of a finite element

Due to the axi-symmetric of the brake, a 2D axi-symmetric model is built in the commercial software ANSYS. The magnetic flux density of the brake using of plane 13 with an applied current of 1.2A is shown in Fig. 16. As shown, the suggested coils' location leads to more uniform magnetic flux in the gap with respect to the locations that are suggested in the previous studies. Fig. 16 also is shown that the maximum values of 0.45T and 1.4T are reached in the drum and MR-fluid gap, respectively.

Because the selected material in the damper and prevent the creation of a permanent magnet in the body, the maximum current of 1.2A can be applied to the system. By applying the maximum current, the value of 0.45T and 1.4T are generated in the steel body (rotor and stator) and MR-fluid gap, respectively. The generated magnetic flux densities are less than the saturated values in the Fig. 14. Because the saturated values lead to higher off-state torque which is not desired. The influence of the arc radius on the output torque at 1.2A using of Table 2 is shown in Fig. 17. The result presents that the output torque increases when the arc radius increase.

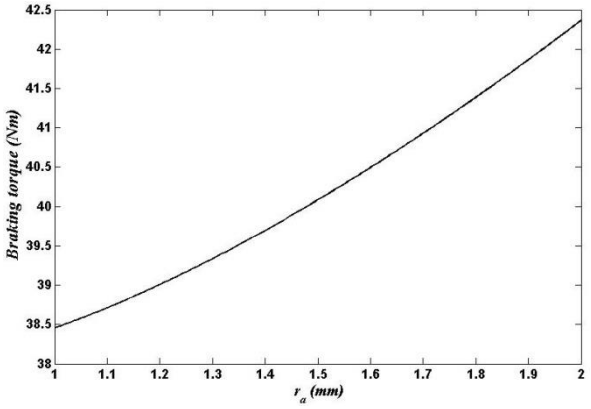

Fig. 17 Relationship of the braking torque and the radius of the arc

Table 2 Parameters of the MR brake to influence of the arc radius

Parameter	Value	Parameter	Value
r_2+r_a	35 mm	r_i	7 mm
d	0.4 mm	r_2	33.5 mm
z	24 mm	W	49 mm

Table 3 Parameters of the MR brake to influence of the gap

Parameter	Value	Parameter	Value
r_2+r_a	35 mm	r_i	7 mm
d	0.4 mm	r_a	1.5 mm
z	24 mm	W	50 mm

The relationship between the MR gap and the output torque at 1.2A using of Table 3 is shown in Fig. 18. The tendency of the output torque decreases when increasing the size of this gap. It shows that the ability to compress the MR block decreases when the MR fluid can move to the gap easily and the magnetic field through this gap also decreases. The conventional MR brake has more decreasing rate with respect to the proposed MR brake. Also the figure shown, with the same gap, the proposed MR brake has more braking torque than the conventional MR brake.

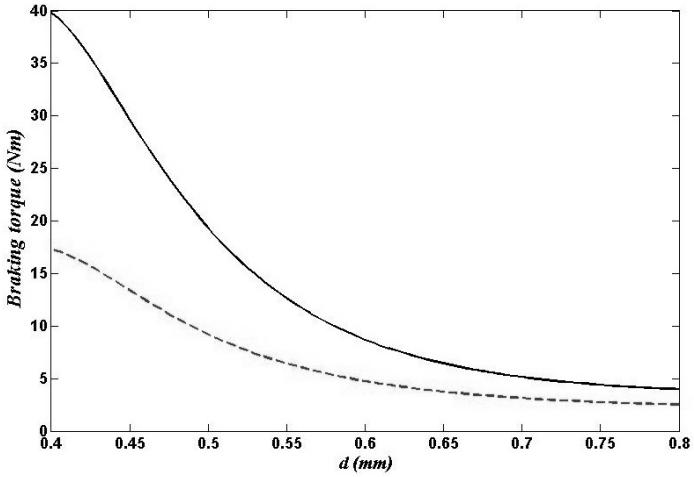

Fig. 18 Relationship of the braking torque and the MR gap. Solid line is the proposed MR brake; dashed line is conventional MR brake

Table 4 Parameters of the MR Brake

Parameter	Value	Parameter	Value
R_o	35.4 mm	r_o	32 mm
R_1	31.6 mm	r_i	7 mm
d	0.4 mm	r_2	33.5 mm
z	24 mm	W	50 mm

With the suggested application, if the design parameters are chosen as in Table 4, the output torque can be achieved about 40 Nm. In this paper, just the typical values are suggested. How to choose the optimal values with optimization process will be calculated in the further researches.

Fig. 19 shows the comparison between the output torque of the proposed MR brake and conventional MR brake with suggested parameters in Table 2. This simulation presents the form of the output torque response respected to the input current. These results also demonstrate the great progress of the proposed MR brake's resistance torque compare with the conventional MR brake.

To validate the presented formulations, the output torque from the proposed MR brake is compared with the formulations which presented in (Nam *et al.* 2009, Nguyen *et al.* 2011) to obtain the generated torque in the outer and the inner faces of the T-flange respectively (Fig. 20). The figure exhibits a good agreement between proposed method and its validation.

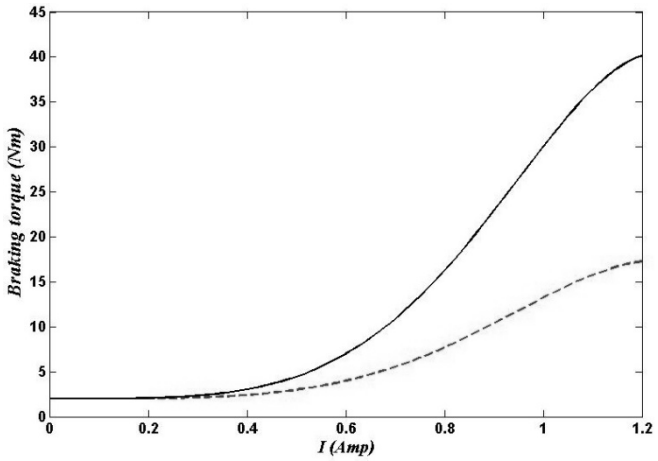

Fig. 19 Simulation results of the braking torque versus the input current. Solid line is the proposed MR brake; dashed line is conventional MR brake

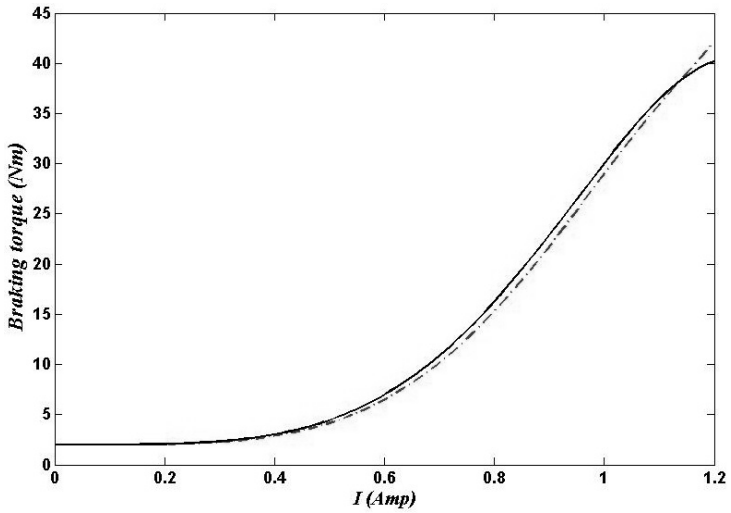

Fig. 20 Braking torque-input current characteristic of the MR brake. Solid line is the proposed method; dashed-dotted line is validation method

8. Conclusions

This study is tried to develop a new configuration MR brake damper incorporating an arc form boundary as prosthetic knee with one disc to achieve desired braking torque. The proposed knee uses magnetic fields to vary the viscosity of the MR fluid to generate the required torque for appropriate flexion/extension resistance. Radial and axial flux directions are used as the hybrid concept to promote achievable torque. Therefore, for this purpose a novel configuration of a T-shaped drum is considered. In current research, Newton's equation of motion is applied for the case of an MR fluid confined between two concentric cylinders to obtain the governing equation of motion of MR fluid in the inner face of the drum to calculate generated torque. The suggested coils' location leads to more uniform magnetic flux in the gap with respect to the locations that are suggested in the previous studies.

The operation mode of an MR fluid in the proposed structure is different from the conventional shear, valve or squeeze film modes. In this design, the T-shaped disc increased effective areas and crushes the particles chains (fibrils) of the MR fluid together. The result of the proposed method is verified with the previous method and validated with the conventional brake under the same input conditions. The generated braking torque by the new disk is greater than that by the conventional one by almost two times.

Acknowledgments

The authors would like to express their gratitude to the Sharif University of Technology for the provided support for this research.

References

Avraam, M., Horodinca, M., Romanescu, I. and Preumont, A. (2010), "Computer controlled rotational MR-brake for wrist rehabilitation device", *J. Intell. Mat. Syst. Str.*, **21**(15), 1543-1557.

Carlson, J.D. and Jolly, M.R. (2000), "MR fluid, foam and elastomer devices", *Mechatronics*, **10**(4), 555-569.

Carlson, J.D., Matthis, W. and Toscano, J.R. (2001), "Smart prosthetics based on magnetorheological fluids", *Smart Struct. Mater.*, **4332**(308), 308-316.

Dyke, S.J., Spencer, B.F. and Sain, M.K. (1998), "An experimental study of MR dampers for seismic protection", *Smart Mater. Struct.*, **7**(5), 693-704.

Gudmundsson, K.H., Jonsdottir, F., Thorsteinsson, F. and Gutfleisch, O. (2011), "An experimental investigation of unimodal and bimodal magnetorheological fluids with an application in prosthetic devices", *J. Intell. Mat. Syst. Str.*, **22**(6), 539-549.

Harnoy, A. (2002), *Bearing Design in Machinery: Engineering Tribology and Lubrication*, Marcel Dekker, Inc., New York, NY, USA.

Hosford, W.F. and Caddell, R.M. (2007), *Metal Forming: Mechanics and Metallurgy*, (3rd Ed.), Cambridge University Press, UK.

Jonsdottir, F., Thorarinsson, E.T., Palsson, H. and Gudmundsson, K.H. (2009), "Influence of parameter variations on the braking torque of a magnetorheological prosthetic knee", *J. Intell. Mat. Syst. Str.*, **20**(6) 659-667.

Jonsdottir, F., Thorarinsson, E.T. and Gutfleisch, O. (2010), "Rheology of perfluorinated polyether-based MR fluids with nanoparticles", *J. Intell. Mat. Syst. Str.*, **21**(11), 1051-1060.

Kirkwood, R.N., Gomes, H.A., Sampaio, R.F., Culham, E. and Costigan, P. (2007), "Biomechanical analysis of hip and knee joints during gait in elderly subjects", *Acta Ortop. Bras.*, **15**(5), 267-271.

Li, W.H. and Du, H. (2003), "Design and experimental evaluation of a magnetorheological brake", *Int. J. Adv. Manuf. Technol.*, **21**(7), 508-515.

Liu, B., Li, W.H., Kosasih, P.B. and Zhang, X.Z. (2006), "Development of an MR-brake-based haptic device", *Smart Mater. Struct.*, **15**(6), 1960-1966.

Naito, H., Akazawa, Y., Tagaya, K., Matsumoto, T. and Tanaka, M. (2009), "An ankle-foot orthosis with a variable-resistance ankle joint using a magnetorheological-fluid rotary damper", *J. Biomech. Sci. Eng.*, **4**(2), 182-191.

Nam, T.H. and Ahn, K.K. (2009), "A new structure of a magnetorheological brake with the waveform boundary of a rotary disk", *Smart Mater. Struct.*, **8**(11), doi:10.1088/0964-1726/18/11/115029.

Nguyen, Q.H. and Choi, S.B. (2011), "A new approach to magnetic circuit analysis and its application to the optimal design of a bi-directional magnetorheological brake", *Smart Mater. Struct.*, **20**(12), doi:10.1088/0964-1726/20/12/125003.

Nguyen, Q.H. and Choi, S.B. (2012a), "Selection of magnetorheological brake types via optimal design considering maximum torque and constrained volume", *Smart Mater. Struct.*, **21**(1), doi:10.1088/0964-1726/21/1/015012.

Nguyen, Q.H. and Choi, S.B. (2012b), "Optimal design of a novel hybrid MR brake for motorcycles considering axial and radial magnetic flux", *Smart Mater. Struct.*, **21**(5), doi:10.1088/0964-1726/21/5/055003.

Park, E.J., Luz, L.F. and Suleman, A. (2008), "Multidisciplinary design optimization of an automotive magnetorheological brake design", *Comput. Struct.*, **86**(3-5), 207-216.

Pinkus, O. and Sternlicht, B. (1961), *Theory of Hydrodynamic Lubrication*, McGraw-Hill, New York, NY, USA.

Rossa, C., Jaegy, A., Micaelli, A. and Lozada, J. (2014), "Development of a multilayered wide-ranged torque magnetorheological brake", *Smart Mater. Struct.*, **23**(2), doi:10.1088/0964-1726/23/2/025028.

Spencer, B.F., Dyke, S.J., Sain, M.K. and Carlson, J.D. (1997), "Phenomenological Model for Magneto-rheological Dampers", *J. Eng. Mech.*, **123**(3), 230-238.

Wereley, N.M., Cho, J.U., Choi, Y.T. and Choi, S.B. (2008), "Magnetorheological dampers in shear mode", *Smart Mater. Struct.*, **17**(1), doi:10.1088/0964-1726/17/01/015022.

Xu, Z.D., Jia, D.H. and Zhang, X.C. (2012), "Performance tests and mathematical model considering magnetic saturation for magnetorheological damper", *J. Intell. Mat. Syst. Str..*, **23**(12), 1331-1349.

Zareh, S.H., Sarrafan, A., Jahromi, A.F. and Khayyat, A. (2011), "Linear quadratic Gaussian application and clipped optimal algorithm using for semi active vibration of passenger car", *Proceedings of the 2011 IEEE International Conference Mechatronics*, Istanbul, Turkey, April.

Zite, J.L., Ahmadkhanlou, F., Neelakantan, V.A., Washington, G.N. and Gregory, N. (2006), "A magnetorheological fluid based orthopedic active knee brace", *Smart Struct. Mater.*, (6171), doi:10.1117/12.658693.

Zhou, Z., Meng, S., Wu, J. and Zhao, Y. (2012), "Semi-active control on long-span reticulated steel structures using MR dampers under multi-dimensional earthquake excitations", *Smart Struct. Syst.*, **10**(6), 557-572.

CY